Supplementary Material for

Imaging spin-wave damping underneath metals using electron spins in diamond

Iacopo Bertelli, Brecht G. Simon, Tao Yu, Jan Aarts, Gerrit E. W. Bauer, Yaroslav M. Blanter & Toeno van der Sar

Correspondence should be addressed to: T.vanderSar@tudelft.nl.

This PDF file includes:

Supplementary Text

Fig. S1-S3

References (*1-4*)

Supplementary Text

1 Eddy-current contribution to spin-wave damping

In this section we derive the additional spin-wave damping caused by the spin-wave-induced eddy currents in a nearby metallic layer. We use the Landau-Lifshitz-Gilbert (LLG) equation to evaluate the various components of the effective magnetic field and find solutions in the absence of additional damping. Then, we evaluate the spin-wave field inside the metal, derive the eddy currents excited by that field, and calculate the additional field component that acts back on the spin-waves, leading to an expression for the effective damping. Last, we consider the finite

width of the metal film in the y direction and include this into the effective damping result.

We consider a thin film of a magnetic insulator (i.e. YIG) in the yz plane, between $-t < x < 0$, with unit magnetization $\mathbf{m}(\mathbf{r})$ oriented along z in equilibrium and saturation magnetization M_s. The bias magnetic field is applied along z. The system is translationally invariant along z.

1.1 LLG equation

The LLG equation is [1]

$$\dot{\mathbf{m}} = -\gamma \mathbf{m} \times [\mathbf{B}_{\text{eff}} + \mathbf{B}_{\text{AC}}] - \alpha \dot{\mathbf{m}} \times \mathbf{m}, \tag{1}$$

where $\mathbf{B}_{\text{AC}}$ is the microstrip magnetic field, γ is the gyromagnetic ratio, α is the Gilbert damping and the effective magnetic field is

$$B_{\text{eff},\alpha} = -\frac{1}{M_s}\frac{\partial F}{\partial m_\alpha}, \tag{2}$$

where $\alpha = x, y, z$. We will now evaluate the various components of the effective magnetic field. We will assume that the spin-wavelength is much larger than the film thickness ($kt \ll 1$) such that we can approximate the magnetization to be homogeneous across the film thickness.

The free energy density includes contributions from the external field $\mathbf{B}_0$, the demagnetizing field $\mathbf{B}_{\text{d}}$, and the exchange interaction:

$$F = -M_s \mathbf{m} \cdot (\mathbf{B}_0 + \mathbf{B}_d/2) + \frac{D}{2} \sum_{\alpha,\beta=x,y,z} \left(\frac{\partial m_\alpha}{\partial \beta}\right)^2, \tag{3}$$

with D the spin stiffness. We define, for convenience, $\omega_B = \gamma B_0$, $\omega_M = \gamma \mu_0 M_s$, and $\omega_D = \frac{\gamma D}{M_s}$.

1.2 Evaluating the contributions to the effective magnetic field

1.2.1 Zeeman energy

The Zeeman energy associated with the external magnetic field $\mathbf{B}_0 = \omega_B \hat{\mathbf{z}}/\gamma$ is

$$F_z = -M_s \mathbf{m} \cdot \mathbf{B}_0. \tag{4}$$

1.2.2 Exchange energy

The exchange energy density in YIG is isotropic

$$F_{\text{ex}}(\mathbf{r}) = \frac{D}{2} \sum_{\alpha,\beta=x,y,z} \left(\frac{\partial m_\alpha(\mathbf{r})}{\partial \beta} \right)^2 . \tag{5}$$

Its Fourier transform over the in-plane coordinates y, z is:

$$F_{\text{ex}}(\mathbf{k}, x) = -k^2 D(m_y^2(\mathbf{k}, x) + m_z^2(\mathbf{k}, x)) + \frac{D}{2} \sum_{\alpha=x,y,z} \left(\frac{\partial m_\alpha(\mathbf{k}, x)}{\partial x} \right)^2 . \tag{6}$$

For a constant magnetization over the film thickness, the exchange energy contributes an effective field with Cartesian components:

$$B_{\text{D},\alpha} = -\frac{1}{M_s} \frac{\partial F}{\partial m_\alpha} = -\frac{\omega_D}{\gamma} k^2 m_\alpha(\mathbf{k}, x). \tag{7}$$

1.2.3 Demagnetizing field

The magnetic field generated by a magnetization $M_s \mathbf{m}(\mathbf{r})$ is given by [2]:

$$\mathbf{B}(\mathbf{r}) = \mu_0 M_s \int \Gamma(\mathbf{r} - \mathbf{r}') \mathbf{m}(\mathbf{r}') d\mathbf{r}', \tag{8}$$

where $\Gamma(\mathbf{r} - \mathbf{r}')$ is the real-space dipolar tensor, with components that are derivatives of the "Coulomb kernel":

$$\Gamma_{\alpha\beta}(\mathbf{r}) = \frac{\partial^2}{\partial\alpha\partial\beta} \frac{1}{4\pi|\mathbf{r}|}, \quad \text{with} \quad \alpha, \beta = x, y, z. \tag{9}$$

The 2D Fourier transform of Eq. (8) is [1]:

$$\mathbf{B}(\mathbf{k}, x) = \mu_0 M_s \int \Gamma(\mathbf{k}, x - x') \mathbf{m}(\mathbf{k}, x') dx', \tag{10}$$

where $\mathbf{k} = (k_y, k_z)$ and with magnetization

$$\mathbf{m}(\mathbf{r}) = \begin{cases} \mathbf{m}(y, z) & \text{for } -t < x < 0 \\ 0 & \text{elsewhere} \end{cases} . \tag{11}$$

[1] We define $g(k_x) = \int g(x) e^{-ik_x x} dx$ and $g(x) = \frac{1}{2\pi} \int g(k_x) e^{ik_x x} dk_x$

The demagnetizing field, averaged over the film thickness, is given by:

$$\overline{\mathbf{B}}(\mathbf{k}) = \mu_0 M_s \frac{1}{t} \int_{-t}^{0} \int_{-t}^{0} \Gamma(\mathbf{k}, x - x') dx' dx \mathbf{m}(\mathbf{k}) = \mu_0 M_s \overline{\Gamma}(\mathbf{k}) \mathbf{m}(\mathbf{k}), \tag{12}$$

where the overline indicates averaging over the thickness. The components of the dipolar tensor in Fourier space are:

$$\Gamma_{\alpha\beta}(\mathbf{k}, x) = \frac{1}{2} \begin{cases} e^{-k|x|} k - 2\delta(x) & \text{for } \alpha = \beta = x, \\ -e^{-k|x|} \frac{k_\alpha k_\beta}{k} & \text{for } \alpha, \beta = y, z, \\ -e^{-k|x|} \text{sign}(x) i k_\alpha & \text{for } \alpha = y, z \text{ and } \beta = x. \end{cases} \tag{13}$$

Using

$$\frac{1}{t} \int_{-t}^{0} \int_{-t}^{0} e^{-k|x-x'|} dx' dx = \frac{2}{k} (1 - \frac{1 - e^{-kt}}{kt}) = \frac{2}{k} f(kt), \tag{14}$$

$$\frac{1}{t} \int_{-t}^{0} \int_{-t}^{0} \text{sign}(x - x') e^{-k|x-x'|} dx' dx = 0, \tag{15}$$

$$\frac{1}{t} \int_{-t}^{0} \int_{-t}^{0} \delta(x - x') dx' dx = 1, \tag{16}$$

we arrive at

$$\overline{\mathbf{B}}(\mathbf{k}) = \mu_0 M_s \begin{pmatrix} f(kt) - 1 & 0 & 0 \\ 0 & \frac{-k_y^2}{k^2} f(kt) & \frac{-k_y k_z}{k^2} f(kt) \\ 0 & \frac{-k_y k_z}{k^2} f(kt) & \frac{-k_z^2}{k^2} f(kt) \end{pmatrix} \begin{pmatrix} m_x(\mathbf{k}) \\ m_y(\mathbf{k}) \\ m_z(\mathbf{k}) \end{pmatrix}, \tag{17}$$

with $f(kt) \to kt/2$ for $kt \ll 1$.

1.3 Spin-wave susceptibility

The linearized Eq. (1) in the frequency domain reads:

$$-i\omega m_x = -\gamma (B_z m_y - B_y) + i\alpha\omega m_y, \tag{18}$$

$$-i\omega m_y = -\gamma (B_x - B_z m_x) - i\alpha\omega m_x. \tag{19}$$

Using $\mathbf{B} = \mathbf{B}_{\text{eff}} + \mathbf{B}_{\text{AC}}$ and with $\Gamma_{xy} = \Gamma_{yx} = 0$ (from Eq. (17)) we obtain

$$\gamma B_x = \omega_M (f-1) m_x - \omega_D k^2 m_x + \gamma B_{\text{AC},x}, \tag{20}$$

$$\gamma B_y = -\omega_M f \sin^2\phi m_y - \omega_D k^2 m_y + \gamma B_{\text{AC},y}, \tag{21}$$

$$\gamma B_z = \omega_B, \tag{22}$$

where ϕ is the angle between the wave vector $\mathbf{k}$ and $\mathbf{B}_{\text{eff}}$. With

$$\omega_0 = \omega_B + \omega_D k^2, \tag{23}$$

$$\omega_2 = \omega_0 + \omega_M (1-f), \tag{24}$$

$$\omega_3 = \omega_0 + \omega_M f \sin^2\phi, \tag{25}$$

we obtain Eqns. (18-19) in matrix form:

$$\begin{pmatrix} \omega_2 - i\alpha\omega & i\omega \\ -i\omega & \omega_3 - i\alpha\omega \end{pmatrix} \begin{pmatrix} m_x \\ m_y \end{pmatrix} = \gamma \begin{pmatrix} B_{AC,x} \\ B_{AC,y} \end{pmatrix}. \tag{26}$$

Inverting Eq. (26) gives the susceptibility

$$\chi = \frac{\gamma}{(\omega_2 - i\alpha\omega)(\omega_3 - i\alpha\omega) - \omega^2} \begin{pmatrix} \omega_3 - i\alpha\omega & -i\omega \\ i\omega & \omega_2 - i\alpha\omega \end{pmatrix}. \tag{27}$$

It is singular when:

$$\Lambda = (\omega_2 - i\alpha\omega)(\omega_3 - i\alpha\omega) - \omega^2 = 0. \tag{28}$$

The real parts of the solutions of this quadratic equation give the spin wave dispersion $\omega_{sw} = \sqrt{\omega_2 \omega_3}$, plotted in Fig. 3c of the main text. In Fig. 3c, the solid lines indicate the dispersion for spin waves propagating along $\pm z$ (i.e., $\phi = 0$ and $\phi = \pi$) and along $\pm y$ (i.e., $\phi = \pm\pi/2$). The spin-wave linewidth $\alpha(\omega_2 + \omega_3)/2$ follows from the imaginary part of Eq. (28), and the ellipticity of the magnetization precession is given by

$$\eta = \left| \frac{\chi_{xx}}{\chi_{yx}} \right|_{(\omega = \omega_{sw})} = \sqrt{\frac{\omega_3}{\omega_2}}. \tag{29}$$

Applying the bias field B_0 along $\theta_{B_0} = 34^\circ$ as in the experiments changes $\omega_0 \rightarrow \omega_B \cos\theta_{B_0} + \omega_D k^2$, but does not introduce additional terms in the susceptibility for B_0 much smaller than the demagnetizing field ($B_0 \ll \mu_0 M_s$), as in this work.

1.4 Eddy-current-induced spin-wave damping

In this section, we introduce the field generated by eddy currents into the LLG equation. We first derive the eddy currents in a metal film (parallel to the yz plane and located between $0 < x < h$) induced by the spin-wave stray field. The eddy currents in turn generate a magnetic field $\mathbf{B}_e$ that couples back into the LLG equation, which should be solved self-consistently. We focus on spin waves travelling in the $+y$-direction, such that $k = k_y$ (thus $\phi = \pi/2$). Our films are much thinner than the magnetic skin depth (1.7 μm for gold at 2 GHz) such that the dipolar stray fields are not screened significantly. Because the film is thin, we neglect eddy currents in the out-of-plane direction. The in-plane eddy currents are induced by the out-of-plane component of the magnetic field, given by (see Eq. (13)):

$$\overline{B}_x = \frac{\mu_0 M_s}{2} \frac{1}{h} \int_0^h dx \int_{-t}^0 dx' k e^{-k(x-x')} (m_x - i m_y) \tag{30}$$

$$= \frac{\mu_0 M_s}{2} k t g (m_x - i m_y), \tag{31}$$

where the overbar denotes an average over the metal (h) thickness. Here,

$$g = \frac{(1 - e^{-kh})}{kh} \frac{(1 - e^{-kt})}{kt}. \tag{32}$$

For an infinitely thin film, $g \rightarrow 1$. From Faraday's law, $\overline{B}_x$ generates a charge current :

$$J_z = \sigma E_z = \sigma \frac{\omega}{k_y} \overline{B}_x = \omega \frac{\sigma \mu_0 M_s t}{2} g (m_x - i m_y), \tag{33}$$

where σ is the conductivity and E_z the electromotive force. As we will further discuss in 1.6, this equation is valid in the limit $kw \gg 1$, with w the width of the film, since we used a Fourier transform over y and did not specify boundary conditions. In Fig. 2d of the main text, $w = 20$ μm and $\lambda < 9$ μm, such that $kw > 14$.

1.4.1 Field generated by the eddy currents

The current J_z generates a field $\mathbf{B}_e$ inside the YIG film. Its average over the YIG thickness is

$$\overline{B}_{e,x} = i\frac{\mu_0 J_z h}{2} g = i\omega \frac{\mu_0^2 M_s \sigma}{4} th \cdot g^2 (m_x - i m_y), \tag{34}$$

$$\overline{B}_{e,y} = i\overline{B}_{e,x}, \tag{35}$$

which we can rewrite as

$$\gamma \overline{B}_{e,x} = i\omega \alpha_m (m_x - i m_y), \tag{36}$$

$$\gamma \overline{B}_{e,y} = -\alpha_m \omega (m_x - i m_y), \tag{37}$$

where

$$\alpha_m = \gamma \frac{\mu_0^2 M_s \sigma}{4} th \cdot g^2 \tag{38}$$

is a dimensionless factor that turns out to be the eddy current contribution to the damping as discussed in the next section. Because the equation was derived under the approximation of a homogeneous magnetization across the film thickness it is valid in the thin-film limit $kt, kh \ll 1$ where $g^2(k) \to 1 - k(t+h)$. The factor $g^2(k)$ arises from averaging the dipolar and eddy current stray fields over the thicknesses of the metal and magnet films. Including a non-homogeneous magnetization across the film thickness may be achieved via micromagnetic simulations. In Fig. 2d of the main text, $0.16 < kt < 0.37$ (for $4\ \mu\text{m} < \lambda < 9\ \mu\text{m}$.)

1.5 Solutions to the LLG equations with eddy currents

We now incorporate $\mathbf{B}_e$ into the LLG equation by adding it to Eqs. (20-22) for $\phi = \pi/2$

$$\gamma B_x = -(\omega_M (1-f) + \omega_D k^2) m_x + \alpha_m \omega \left(i m_x + m_y\right) + \gamma B_{AC,x}, \tag{39}$$

$$\gamma B_y = -(\omega_M f + \omega_D k^2) m_y - \alpha_m \omega \left(m_x - i m_y\right) + \gamma B_{AC,y}, \tag{40}$$

$$\gamma B_z = \omega_B. \tag{41}$$

The linearized LLG equations (18-19) become

$$-i\omega m_x = -(\omega_3 - i(\alpha+\alpha_m)\omega)m_y - \alpha_m\omega m_x + \gamma B_{AC,y}, \tag{42}$$

$$-i\omega m_y = (\omega_2 - i(\alpha+\alpha_m)\omega)m_x - \alpha_m\omega m_y - \gamma B_{AC,x}, \tag{43}$$

where ω_2 and ω_3 are given in Eqs. (23-25). In matrix form:

$$\begin{pmatrix} \omega_2 - i(\alpha+\alpha_m)\omega & (i-\alpha_m)\omega \\ -(i-\alpha_m)\omega & \omega_3 - i(\alpha+\alpha_m)\omega \end{pmatrix} \begin{pmatrix} m_x \\ m_y \end{pmatrix} = \gamma \begin{pmatrix} B_{AC,x} \\ B_{AC,y} \end{pmatrix}. \tag{44}$$

The resulting susceptibility is singular when

$$\Lambda = (\omega_2 - i(\alpha+\alpha_m)\omega)(\omega_3 - i(\alpha+\alpha_m)\omega) + (i-\alpha_m)^2\omega^2 = 0. \tag{45}$$

Solving this quadratic equation and disregarding terms of order α^2 leads to

$$\omega = \sqrt{\omega_2\omega_3} - i\left[\alpha_m\sqrt{\omega_2\omega_3} + (\alpha+\alpha_m)\frac{\omega_2+\omega_3}{2}\right]. \tag{46}$$

We observe that including the eddy currents yields the same spin-wave dispersion $\omega_{sw} = \sqrt{\omega_2\omega_3}$, but renormalizes the linewidth according to

$$\alpha\frac{\omega_2+\omega_3}{2} \to \alpha_m\left[\sqrt{\omega_2\omega_3} + \frac{\omega_2+\omega_3}{2}\right], \tag{47}$$

where we assumed $\alpha_m \gg \alpha$. The eddy-current-induced damping can thus be included into Eq. (1) by setting

$$\alpha = \alpha_e = \alpha_m\frac{\sqrt{\omega_2\omega_3} + \frac{\omega_2+\omega_3}{2}}{\frac{\omega_2+\omega_3}{2}} = \alpha_m\frac{(1+\eta)^2}{1+\eta^2}. \tag{48}$$

Substituting Eq. (38) leads to Eq. 1 in the main text. In section 1.7 we find the same expression using an alternative derivation.

1.6 Metal film of finite width

We now consider a metal strip with finite width w along y. The effective orbital magnetization of the eddy currents induced by the spin-wave field points in the x-direction and is determined

by the Maxwell-Faraday equation:

$$\frac{\partial^2 m_z^{eff}}{\partial y^2} = -i\omega\sigma \bar{B}_x(y), \quad \text{with} \quad j_z = -\partial m_z^{eff}/\partial y, \tag{49}$$

where $\bar{B}_x(y)$ is the stray field of a spin wave travelling in the $+y$ direction, Fourier transformed over time but not over coordinates. It is given by (c.f. Eq. (31))

$$\bar{B}_x(y) = \frac{\mu_0 M_s}{2} ktg(m_x - im_y). \tag{50}$$

Introducing the notations $m_{x,y} = m_{x,y}^{(0)} e^{iky}$, the solution of Eq. (49) is

$$m_x^{eff} = \alpha_k \left(e^{iky} - [1 + iky] \frac{\sin \frac{kw}{2}}{\frac{kw}{2}} \right), \tag{51}$$

with

$$\alpha_k = i\omega\sigma \frac{\mu_0 M_s t}{2k} g_k (m_x^0 - i m_y^0). \tag{52}$$

The eddy-current field averaged over the magnetic film thickness, cf. Eq. (34) is:

$$B_{e\alpha}(y) = \frac{1}{t} \int_{-t}^{0} dx B_{e\alpha}(x, y) = \int \frac{dq}{2\pi} B_{e\alpha}(q) e^{iqy}, \tag{53}$$

where

$$B_{e\alpha}(q) = \frac{\mu_0 M_s}{t} \int_{-t}^{0} dx \int_0^h dx' \int_{-\infty}^{\infty} dy dz e^{\prime - iqy} \int_{-w/2}^{w/2} dy' \Gamma_{\alpha x}(\mathbf{r}, \mathbf{r}') m_x^{eff}(\mathbf{r}'). \tag{54}$$

Note that it does not depend on z. Using

$$\int_{-\infty}^{\infty} dy' dz' \frac{e^{iky'}}{\sqrt{(x - x')^2 + y'^2 + z'^2}} = \frac{2\pi}{|k|} e^{-|k(x - x')|}, \tag{55}$$

from Eq. (54) we obtain

$$B_{e\alpha}(q) = \mu_0 M_s \alpha_k |q| h g_{|q|} \left\{ \frac{\sin[(k - q)w/2]}{k - q} - 2 \frac{\sin(qw/2) \sin(kw/2)}{qwk} + \right. \tag{56}$$

$$\left. - \frac{2}{wq^2} \sin \frac{kw}{2} \left[\sin \frac{qw}{2} - \frac{qw}{2} \cos \frac{qw}{2} \right] \right\} \tag{57}$$

and $B_{e,y}(q) = (iq/|q|)B_{e,x}(q)$. In the wide-strip limit $\lim_{w\to\infty} k^{-1}\sin(kw/2) \to \pi\delta(k)$ such that, back in the real-space and time domains,

$$B_{e\alpha}(y,\tau) = \frac{i\omega\sigma\mu_0^2 M_s}{4} e^{-i\omega\tau} th(m_x^0 - im_y^0)(g_k^2 e^{iky} - \frac{2\pi}{w}\delta(k)). \tag{58}$$

The last term reflects that a spatially homogeneous mode does not induce eddy currents. The finite width can be neglected when $kw \gg 1$, in which case we get the same result as Eq. (38). In Fig. 2d of the main text, $kw > 14$.

1.7 Effective magnetic damping

The effective damping parameter can be derived alternatively by equating the magnetic and external energy losses [3]. According to the LLG equation the power density per area of a dynamic magnetization for a scalar Gilbert damping constant reads

$$p^{(m)}(y) = -\int \left(\dot{\mathbf{M}} \cdot \mathbf{B}_{\text{eff}}\right) dx = -\frac{\alpha_{\text{G}} M_s}{\gamma} \int \dot{\mathbf{m}}^2 dx, \tag{59}$$

where the integral is over the magnetic film thickness. In our geometry the power loss density of a spin wave mode $\mathbf{m}_i$ with index i that solves the linearized LLG with frequency ω_i is then

$$p_i^{(m)}(y) = \frac{\alpha_{\text{G}} M_s}{\gamma} \omega_i^2 \int [(m_i^{(x)})^2 + (m_i^{(y)})^2] dx, \tag{60}$$

In the limit $kt \ll 1$, we can replace i by the wave number k of the spin wave in the y direction. The time (τ)-dependent magnetization

$$\mathbf{m}_k = m_k \begin{pmatrix} \eta_k \cos(ky - \omega\tau) \\ \sin(ky - \omega\tau) \end{pmatrix} \tag{61}$$

leads to the time-averaged dissipation

$$p_i^{(m)}(y) = \frac{\alpha_{\text{G}} M_s}{\gamma} \omega_k^2 \frac{1+\eta_k^2}{2} \int m_k^2(x,y)\, dx, \tag{62}$$

We model the energy loss per unit of length under the strip by a phenomenological damping parameter α'_k as

$$P_k^{(m)} = tw\frac{\alpha'_k M_s}{\gamma}\omega_k^2\frac{1+\eta_k^2}{2}\overline{m_k^2}, \tag{63}$$

where the over-bar indicates the spatial average over the film thickness t. Assuming that the magnetic skin depth is much larger than the thickness of the strip h, the stray field averaged over the strip thickness above the film and $k > 0$ reads

$$\bar{B}_x = M_s\mu_0 tk\frac{1+\eta_k}{2}\overline{m_k}\cos\left(ky - \omega\tau\right). \tag{64}$$

This field generates an electromotive force (emf) E_z according to $\partial_y E_z = -\partial_\tau \bar{B}_x$:

$$E_z(y) = -\int_0^y \partial_\tau \bar{B}_x dy' \tag{65}$$

$$= M_s\mu_0 t\frac{1+\eta_k}{2}\overline{m_k}\omega\left[\cos(ky-\omega\tau) - cos(\omega\tau)\right] + \mathrm{C}. \tag{66}$$

The emf does not drive a net charge current since the metal strip is part of a high impedance circuit.

$$J_z = \sigma t\int_0^w E_z(y) = 0 \tag{67}$$

then fixes the integration constant C. The time-averaged ($\langle\cdots\rangle$) integrated Ohmic loss per unit length of the wire then reads

$$P_k^{(\Omega)} = h\sigma\int_0^w \left\langle|E_z|^2\right\rangle dy \tag{68}$$

$$= \sigma\left(\mu_0 t\overline{m_k}\omega\right)^2 hw\left(\frac{2\cos kw + k^2w^2 - 2}{2\left(kw\right)^2}\right). \tag{69}$$

We can now determine the effective damping by setting $P_k^{(\Omega)} \equiv P_k^{(m)}$.

$$\alpha'_k = \gamma M_s ht\sigma\mu_0^2\frac{\overline{m_k}^2}{\overline{m_k^2}}\frac{2\cos kw + k^2w^2 - 2}{2\left(kw\right)^2}\frac{(1+\eta_k)^2}{2(1+\eta_k^2)}. \tag{70}$$

In the long-wavelength and wide-metal-strip regime $w^{-1} \ll k \ll t^{-1}$, $\overline{m_k}^2 \approx \overline{m_k^2}$ and $\eta_k \approx \eta$,

$$\alpha'_e = \gamma M_s ht\sigma\mu_0^2\frac{(1+\eta)^2}{4(1+\eta^2)} \tag{71}$$

agrees with Eq. (48). We note that the scalar α'_m should be interpreted as an appropriate average over the Gilbert damping tensor elements that can be in principle determined by the same procedure.

2 Data fitting procedures

2.1 Extracting the damping from the measured Rabi frequency traces

To fit the measured Rabi frequencies (Fig. 2a-c of the main text) and extract the spin-wave damping, we follow the procedure described in [4]. In this procedure, we first calculate the magnetic field generated by a microwave current in a microstrip propagating along z, given by $\mathbf{B_{AC}} = (B_{AC,x}\hat{\mathbf{x}} + B_{AC,y}\hat{\mathbf{y}})$. We then calculate the resulting magnetization dynamics in Fourier space using $\mathbf{m}(\mathbf{k}) = \chi(\mathbf{k})\mathbf{B}_{\mathrm{AC}}(\mathbf{k})$. From $\mathbf{m}(\mathbf{k})$, we calculate the stray field of the spin waves at the location of the NV sensing layer. We then sum (vectorially) the spin-wave and microstrip fields and calculate the resulting NV Rabi frequency. Free fitting parameters are the microwave current through the microstrip, the spin-wave damping, and a ~ 1 MHz spatially homogeneous offset to account for the field generated by the leads delivering the current to the stripline. In the fitting procedure, we keep fixed the values of the in-plane and out-of-plane angles between the magnetic field and the NV axis, the NV-YIG distance, as well as the thickness and saturation magnetization of YIG. Small uncertainties in their value may explain the small discrepancy between the theoretical and fitted values of the damping under the microstrip at long wavelengths.

Figure S1 shows two example traces calculated using this procedure (red dashed lines) and compares these to a measured trace (blue line) of Fig. 2c of the main text. In both A and B, the calculated traces use a single value of the damping for the entire spatial range. These plots highlight that the measured data in the microstrip region are only described well for a large value of the damping, while the data next to the microstrip are only described well for a low

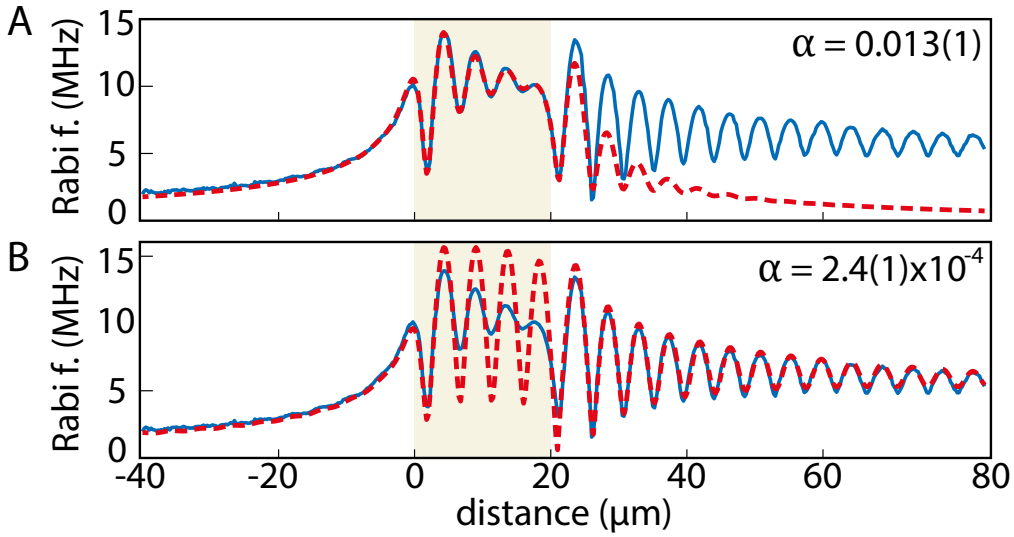

Figure S1. Highlighting the different spin-wave damping underneath and next to the microstrip. Solid blue lines: data trace from Fig. 2c of the main text. Dashed red lines: calculated Rabi frequencies for high (A) and low (B) values of the damping. The calculations use a single value of the damping for the entire spatial range. The high-damping calculation (panel A) only matches the data well in the microstrip region. The low-damping calculation (panel B) only matches the data next to the microstrip. The microstrip is indicated by shaded yellow color.

value of the damping.

2.2 Extracting the damping under the gold structure

To extract the spatial decay length of the spin waves y_{decay} underneath the gold structure from spatial measurements of the ESR contrast $C(y)$ (Fig. 2e-f of the main text and Supplementary Fig. 2) we describe $C(y)$ using

$$C(y) = C_0 \frac{\Omega^2(y)}{\Omega^2(y) + 1}, \tag{72}$$

where C_0 is the known maximum ESR contrast and $\Omega(y)$ is a normalized NV Rabi frequency resulting from the sum of the spin-wave and direct microstrip fields:

$$\Omega(y) = \left| iAe^{i(k(y-y_0)} e^{-(y-y_{\text{struct}})/y_{decay}} + \frac{B}{y - y_0} \right|. \tag{73}$$

Here, y_0 and y_{struct} are the known locations of the edges of the microstrip and gold structure, respectively (see Fig. 2e of the main text), and A, B, and y_{decay} are extracted from the fits. The spatial decay length y_{decay} is given by the linewidth of the susceptibility in k-space and can therefore be related to the damping parameter α by Taylor expanding $\omega_{sw}(k) \approx \omega_{sw}(k_0) + v_g(k - k_0)$ in Eq. (28) to get:

$$\Lambda = 2\omega_{sw}\left(v_g(k - k_0) - i\alpha\frac{\omega_2 + \omega_3}{2}\right). \tag{74}$$

Solving $\Lambda = 0$, we find

$$k = k_0 + i\alpha\frac{\omega_2 + \omega_3}{2v_g}, \tag{75}$$

which yields the relation between the spatial decay length and α

$$y_{decay} = \frac{2v_g}{\alpha(\omega_2 + \omega_3)}, \tag{76}$$

where we calculate ω_2 and ω_3 (defined in Eqs. (24) and (25)) and the spin-wave group velocity v_g from the spin-wave dispersion.

This fit procedure is used to extract the damping from the data in Fig. 2f of the main text, as well as to determine the frequency dependence of the damping underneath the gold structure, for which the data traces and fits are shown in Fig. S2. The extracted values of the damping are plotted in Fig. 2d of the main text.

2.3 Three-magnon scattering threshold

The three-magnon scattering process is enabled for spin waves of frequency at least twice that of the bottom of the spin-wave band ($\omega_{\min}$), which shifts with the applied magnetic field. In the main text, we see this threshold at ∼2.39 GHz (Fig. 3). From the spin-wave dispersion (Eq. (28)), we find that this frequency corresponds to the frequency at which the ω_- NV ESR transition and $2\omega_{\min}$ cross (Fig. S3).

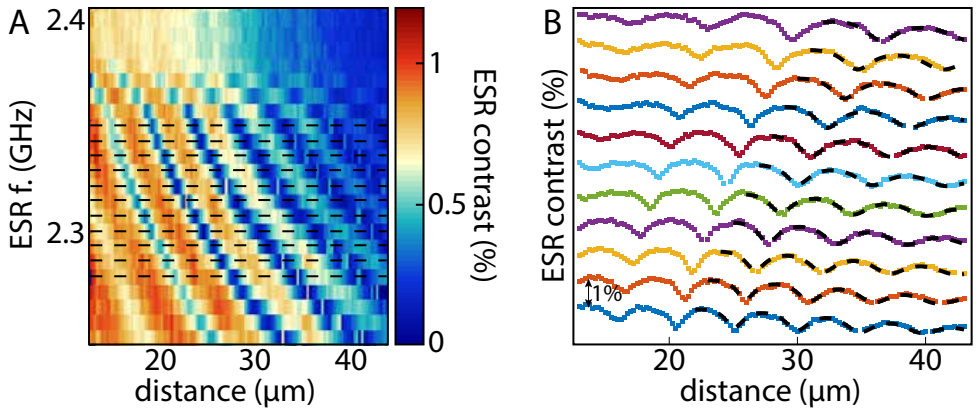

Figure S2. Spin-wave damping under gold structure. (**A**) ESR contrast vs distance for different spin-wave frequencies under the gold structure shown in Fig. 2e of the main text. Dashed black lines: linecuts shown in (B). (**B**) Colored lines: linecuts of (A). Dashed black lines: fits. The fitting range was chosen such that it starts at the first peak for which a decay is visible.

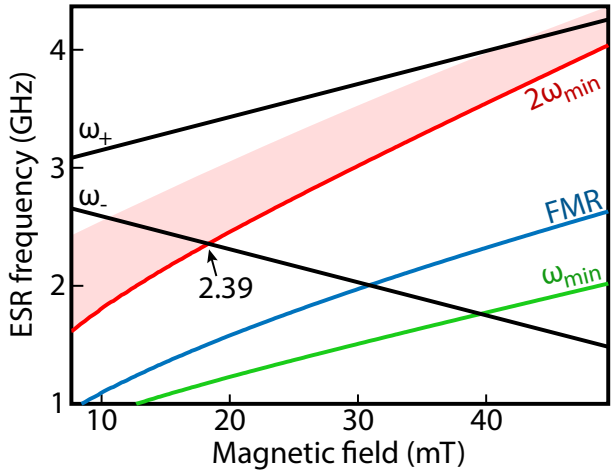

Figure S3. Calculated three-magnon scattering threshold frequency vs magnetic field applied along the NV axis. For frequencies above $2\omega_{\min}$ (shaded red area), scattering of one DE spin wave into two BV waves of frequency close to the band minimum ($\omega_{\min}$, solid green line) becomes possible. Solid black lines (indicated as $\omega_{\pm}$) represent the NV ESR transitions. ω_{-} and $2\omega_{\min}$ cross at a frequency close to 2.39 GHz, as shown in Fig. 3 of the main text. Solid blue line: FMR of YIG.

References

[1] T. L. Gilbert, A phenomenological theory of damping in ferromagnetic materials, *IEEE Transactions on Magnetics* **40**, 3443-3449 (2004).

[2] K. Y. Guslienko, A. N. Slavin, Magnetostatic Green's functions for the description of spin waves in finite rectangular magnetic dots and stripes, *Journal of Magnetism and Magnetic Materials* **323**, 2418 (2011).

[3] A. Brataas, Y. Tservkovnyak, G.E.W. Bauer, Magnetization dissipation in ferromagnets from scattering theory, *Physical Reviews B* **84**, 054416 (2011)

[4] I. Bertelli, J. J. Carmiggelt, T. Yu, B. G. Simon, C. C. Pothoven, G. E. W. Bauer, Y. M. Blanter, J. Aarts, and T. van der Sar, Magnetic resonance imaging of spin-wave transport and interference in a magnetic insulator, *Science Advances* **6**, eabd3556 (2020).